Experimental Investigation of Underwater Optical Wireless Communication for Correlated SIMO Channel Under Temperature-Induced Turbulence

Weijie Liu, Wenli Jiang, Nuo Huang, and Zhengyuan Xu, *Senior Member, IEEE*

***Abstract*—Turbulence is an intractable issue for underwater optical wireless communication (UOWC). In this paper, the effects of temperature-induced turbulence on the UOWC system with correlated single-input multiple-output (SIMO) channel are comprehensively investigated, and the feasibility of employing a detector array in mitigating the turbulence-induced signal fluctuation is experimentally verified. Experimental results show that the spatial diversity can ensure the satisfactory bit error rate (BER) and outage probability performance with the maximum ratio combining (MRC) under correlated turbulence channel. The optimal paired combinations can achieve a signal-to-noise ratio (SNR) gain above 3 dB over the single branch receiver at the BER of 10^{-3}. Moreover, the diversity gain will be reduced by the subchannel correlation when the arrayed receiver elements adopted to mitigate the turbulence effect fail to be placed sufficiently far apart.**

***Index Terms*—Underwater optical wireless communication, correlated SIMO channel, detector array, lognormal fading.**

I. Introduction

UNDERWATER optical wireless communication (UOWC) has become increasingly popular in the last decades thanks to its high data rate and long transmission distance [1], [2], [3], [4], [5], reaching an order of Gigabits per second (Gbps) and hundreds of meters simultaneously. However, the propagation of optical signals in water is seriously affected by various channel effects, such as scattering, absorption, bubbles and turbulence [6], [7], [8].

The characteristics of underwater turbulence channel and their impact on UOWC have been widely investigated from both theoretical and experimental aspects [9], [10], [11], [12], [13], and the spatial receiving diversity is typically leveraged to mitigate channel turbulence. The combination of signals from uncorrelated subchannels can greatly alleviate the impact of turbulence. In [14], a single-input multiple-output (SIMO) spatial diversity reception scheme was proposed to mitigate channel fading under scattering/absorption and underwater turbulence. Jamali et al. analytically derived an exact bit error rate (BER) expression and its upper bound for a multiple-input multiple-output (MIMO) UOWC system with equal gain combining (EGC) and maximum ratio combining (MRC) under turbulence-induced channel fading [15]. A comprehensive experimental investigation about the impact of coding and receiver diversity on the UOWC performance over the turbid and turbulent seawater channel was conducted by Ramavath et al., and a maximum 8 dB power gain was obtained for the system incorporating combining techniques and their proposed Bose-Chaudhuri-Hocquenghem (BCH) code [16]. When the receiver elements fail to be placed sufficiently far apart, the free space subchannel fading becomes correlated, reducing the diversity gain [17], [18], [19], [20]. Zhu et al. proposed a maximum likelihood detection scheme for spatial diversity reception concerning turbulence-induced correlated subchannel fading in time domain [17]. Alouini et al. derived the closed-form expressions for the moments of the output signal-to-noise ratio (SNR) of different combining scheme-based diversity receivers, including dual-branch MRC, selective combining (SC), and switch-and-stay combining (SSC) diversity receivers operating over correlated Lognormal (LN) fading channels [18]. In [19], an exact closed-form expression for signal-to-interference ratio (SIR) distribution of a dual antenna system in Rayleigh fading channels is obtained considering channel correlation. Furthermore, the statistical correlation between turbulence influenced optical signals captured by two adjacent spatial receivers was mathematically investigated under a weak turbulence condition [20].

Clearly, existing investigations on the detector array based turbulence mitigation mainly focus on the performance analysis without considering the correlation among subchannels when the detectors fail to be placed sufficiently far apart. This paper presents various experimental results of the UOWC system with multiple detectors operated under temperature-induced turbulence channel with subchannel correlations. The system model and the derivations of statistical MRC weights in the presence of both the turbulence-induced channel fading and the subchannel correlations are briefly provided. Then, the experimental setup is introduced to further verify the feasibility of the detector array based turbulence mitigation method and the derived combining weights. The experimental results suggest that stronger correlation between subchannels will lead to smaller combining

Manuscript received 24 March 2023; revised 21 May 2023; accepted 23 June 2023. Date of publication 27 June 2023; date of current version 5 July 2023. This work was supported in part by the National Key Research and Development Program of China under Grant 2022YFB2903400, in part by the Strategic Priority Research Program of CAS under Grant XDA22000000, and in part by the National Natural Science Foundation of China under Grant 62101526. *(Weijie Liu and Wenli Jiang are co-first authors.) (Corresponding authors: Nuo Huang; Zhengyuan Xu.)*

The authors are with the CAS Key Laboratory of Wireless-Optical Communications, School of Information Science and Technology, University of Science and Technology of China, Hefei 230027, China (e-mail: lwj1993@ustc.edu.cn; jwl1998@mail.ustc.edu.cn; huangnuo@ustc.edu.cn; xuzy@ustc.edu.cn).

Digital Object Identifier 10.1109/JPHOT.2023.3289797

gain. To the best of our knowledge, this is the first time that UOWC link correlation is experimentally investigated under the temperature-induced turbulence and channel fading, which provides guidance for the transmission design in practical UOWC systems.

II. MRC Under Channel Correlation

For an no-return-to-zero on-off keying (NRZ-OOK) based UOWC system, the transmitted optical signal can be denoted as sP, where s is the binary bit taking 0 and 1 with equal probability, P is the maximum optical power. After the modulated light passes through a turbulence channel with correlation across outputs of multiple detectors, the output electrical signal of the i-th avalanche photodiode (APD) detector $(i = 1, \ldots, N)$ ignoring the background irradiance can be expressed as

$$r_i = sPh_i\eta_i g_i + n_t, \tag{1}$$

where h_i with mean μ_i and variance σ_i^2 is the random channel gain between the optical source and the i-th APD detector, and the correlation coefficient between h_i and h_j is denoted by ρ_{ij}; η_i and g_i are the quantum efficiency and internal gain of the i-th APD detector, respectively; n_t represents the Gaussian noise with zero mean and variance σ_t^2 [21]. For analytical simplicity and without loss of generality, the quantum efficiencies of all APDs are assumed to be $\eta_1 = \cdots = \eta_N = 1$.

Given the combining weight vector $\mathbf{w}$ of the N detector branches, the combined signal can then be written as

$$y = sP\mathbf{w}^T\mathbf{G}\mathbf{h} + \mathbf{w}^T\mathbf{n}_t, \tag{2}$$

where the column vectors $\mathbf{h}$ and $\mathbf{n}_t$ collect instantaneous channel gains and thermal noises for N branches respectively, superscript $\mathbf{T}$ represents transpose, $\mathbf{G} = diag(\mathbf{g})$ is the diagonal matrix whose diagonal elements are the elements of APD gain vector $\mathbf{g} = [g_1, \ldots, g_N]^T$. Since the instantaneous channel gain vector $\mathbf{h}$ for detector array cannot be acquired in practical implementation, the average SNR of the combiner output can then be defined as

$$\gamma_y = \frac{\frac{P^2}{2}\mathbb{E}(\mathbf{w}^T\mathbf{G}\mathbf{h}\mathbf{h}^T\mathbf{G}^T\mathbf{w})}{\mathbf{w}^T\left(\sigma_t^2\mathbf{I}\right)\mathbf{w}} = \frac{P^2}{2\sigma_t^2}\frac{\mathbf{w}^T\mathbf{R}\mathbf{w}}{\mathbf{w}^T\mathbf{w}}, \tag{3}$$

where $\mathbb{E}(\cdot)$ denotes the expectation operation, and $\mathbf{R}$ is the correlation matrix with the (i, j)-th element as $g_i g_j(\rho_{ij}\sigma_i\sigma_j + \mu_i\mu_j)$.

The objective of the MRC scheme is to find the optimal weight vector $\mathbf{w}$ which maximizes the average SNR under channel fading. Obviously, (3) is in the form of Rayleigh quotient, and the MRC weight vector $\mathbf{w}$ can be readily solved as the eigenvector of matrix $\mathbf{R}$ corresponding to its maximum eigenvalue $\lambda_{\max}$.

III. Experimental Setup and Details

Fig. 1 shows a block diagram of the experimental UOWC system employing a spatial diversity detector and NRZ-OOK modulation scheme, and Fig. 2 presents the corresponding experimental setup.

At the transmitter (Tx), a 2^{14} pseudo-random binary sequence (PRBS) with 10 times upsampling is generated in MATLAB and further loaded to an arbitrary waveform generator (AWG)

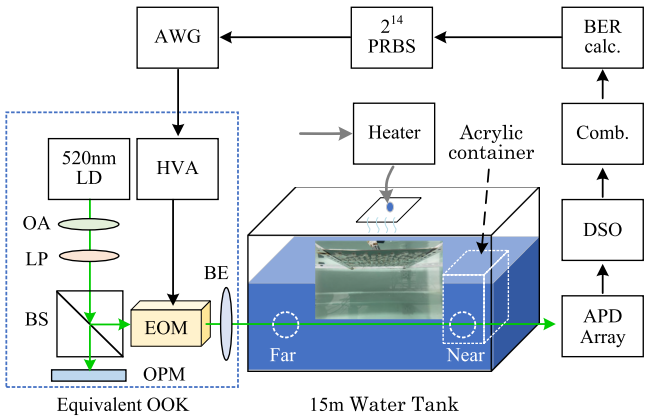

Fig. 1. Block diagram of the experimental spatial diversity detector based UOWC system.

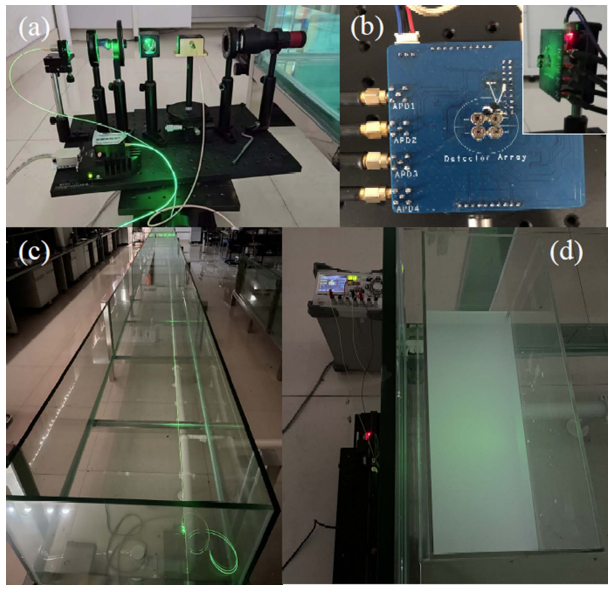

Fig. 2. Experimental setup with (a) equivalent OOK transmitter, (b) self-designed APD array, (c) 15 m-long water tank, (d) transparent acrylic container filled with turbid water in front of the detector array.

(Keysight, 33612 A) sampling at 6.25 MSa/s. A polarization based external modulation is employed to achieve an equivalent OOK scheme with 100% modulation depth [22]. A horizontal linear polarizer (LP) (Thorlabs, WP25MVIS) is adopted after a single-mode pigtailed 520 nm laser diode (LD) (Thorlabs, LP520-SF15) equipped with a fixed focus collimators (Thorlabs, F220FC-532), to facilitate acquisition of a completely horizontally polarized light beam. An adjustable optical attenuator (OA) is placed after the LP to facilitate precise adjustment of the total emitted optical power. A beam splitter (BS) associated with an optical power meter (OPM) is used to monitor the transmitted optical power. Then, an electro-optical modulator (EOM) (Thorlabs, EO-AM-NR-C4) driven by a high-voltage amplifier (HVA) (Thorlabs, HVA200), whose maximum modulating bandwidth reaches 1 MHz, is employed to change the polarization state of the output light beam according to the transmitted signal from AWG. A beam expander (BE) is used to diffuse the beam and

obtain a larger spot diameter in order to fully cover the area of the detector array.

A water tank with the dimensions of 15 m × 0.8 m × 0.6 m is used to simulate underwater turbulence channel while the depth of remaining tap water is about 0.4 m with initial temperature of 20°C. An outlet panel, which is parallel to the direction of light propagation, is placed below the water surface. A distance of 2 cm between the panel and the light beam is reserved to ensure sufficient space for generation of turbulence. A water heater is used to provide hot water with temperature of 45 °C for generating temperature-induced turbulence channel [10]. An optional acrylic container filled with turbid water will be placed in front of the detector array when we investigate the effect of turbidity on the communication performance over a temperature-induced turbulence channel.

At the receiver (Rx), a self-made detector array with four APDs is used to convert the optical signals into electrical signals. Each detector branch consists of a commercial APD (Hamamatsu, S12053-10), a self-designed high voltage driver and a post amplifier whose 3 dB bandwidth larger than 70 MHz and noise standard derivation less than 1 mV can be obtained under an APD initial gain of 30. An digital storage oscilloscope (DSO) (Tektronix, MSO68B) with four channels sampling at 6.25 MSa/s, is employed to capture the output signal from each APD. The obtained signal after MRC is demodulated for final communication performance evaluation.

IV. Experimental Results and Discussions

In this section, the statistical characteristics following two cases where turbulence occurs at the transmitter and receiver are provided, and the communication performances of the detector array based turbulence mitigation method are analyzed as well.

A. Characteristics of Correlated Turbulence Channel

As shown in Fig. 1, two turbulence channels are achieved by generating the turbulence near and far from the APD array, which are represented by Case 1 and Case 2 in the following, respectively.

Fig. 3 shows the statistical distribution and LN fitting results for temperature-induced turbulence occurring at different locations. Generally, scintillation index (SI) is used to describe the turbulence strength, and larger SI corresponds to stronger turbulence. Obviously, a smaller amplitude and larger SI can be observed for Case 2, which indicates a higher emitted optical power is required for Case 2 to achieve similar communication performance as Case 1. Meanwhile, it can be seen that the LN distribution can well describe the statistical characteristics of received intensity, whose statistical moments will be leveraged in the following MRC scheme to further optimize the communication performances.

To investigate the effect of dispersion, Fig. 4 shows the probability densities of measured channel gains and LN fitting results at different receiving positions from the light spot center till distance of 70 mm away at a step size of 14 mm in Case 2, and the corresponding mean and variance can be summarized in Table I. It can be seen that the mean and variance of the

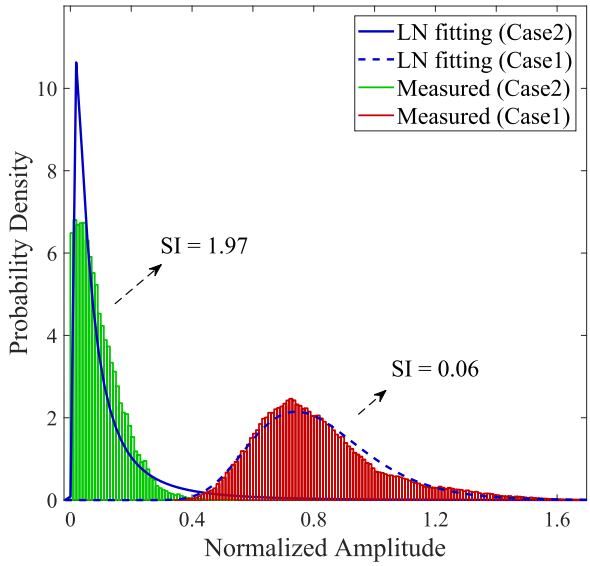

Fig. 3. Statistical distribution of signal intensity for Case 1 with $SI = 0.06$ and Case 2 with $SI = 1.97$.

TABLE I
Mean and Variance of Measured Channel Gains at Different Receiving Positions for Case 2

Offset (mm)	0	14	28	42	56	70
μ (mV)	5.512	6.091	3.482	1.648	0.41	0.4124
σ^2	39.891	57.195	15.960	3.078	0.041	0.0415

channel gain both roughly decrease with the offset distance d, which implies the non-uniform intensity distribution within the light spot. Note that the mean and variance of channel gain at $d = 0$ mm are smaller than those at $d = 14$ mm, which can result from the deviation between the real spot center and test point.

The turbulence-induced fading observed by different detectors becomes correlated when the receiver elements fail to be placed sufficiently far apart at the receiving plane, which reduces the diversity gain when mitigating the turbulence effect in the UOWC system. The channel correlation coefficient matrices corresponding to aforementioned two cases are measured respectively as

$$\mathbf{C}_1 = \begin{bmatrix} 1.00 & 0.16 & 0.11 \\ 0.16 & 1.00 & 0.04 \\ 0.11 & 0.04 & 1.00 \end{bmatrix}, \mathbf{C}_2 = \begin{bmatrix} 1.00 & 0.68 & 0.15 \\ 0.68 & 1.00 & 0.32 \\ 0.15 & 0.32 & 1.00 \end{bmatrix}.$$

Obviously, the latter indicates a strong correlation case, while the former indicates a weak correlation case.

To gain a better understanding of the impact of correlation across multiple detectors, Fig. 5 provides the normalized amplitudes of received signal under three channels corresponding to different detectors, namely subchannel 1 (CH1), subchannel 2 (CH2), and subchannel 3 (CH3). It can be seen that the strong channel correlation leads to a more similar fluctuation trend between CH1 and CH2 as shown in Fig. 5.

Fig. 6 shows the instantaneous light spot on the receiving plane of the APD detector array after traveling through a 15 m-long water tank in Case 1 and Case 2 respectively. Different

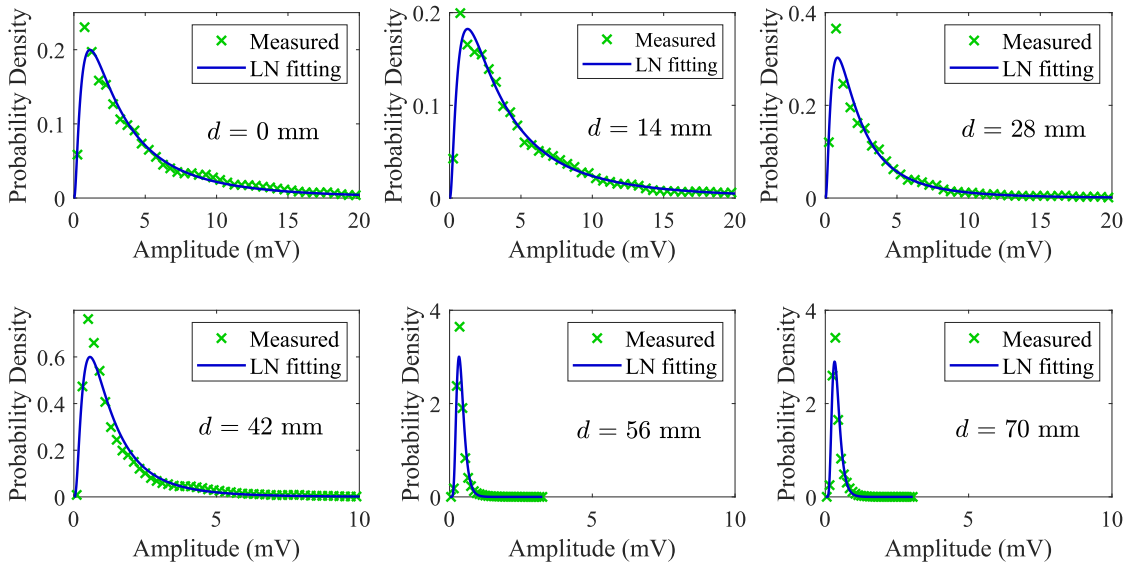

Fig. 4. Probability densities of measured channel gains and LN fitting results at different receiving positions for Case 2.

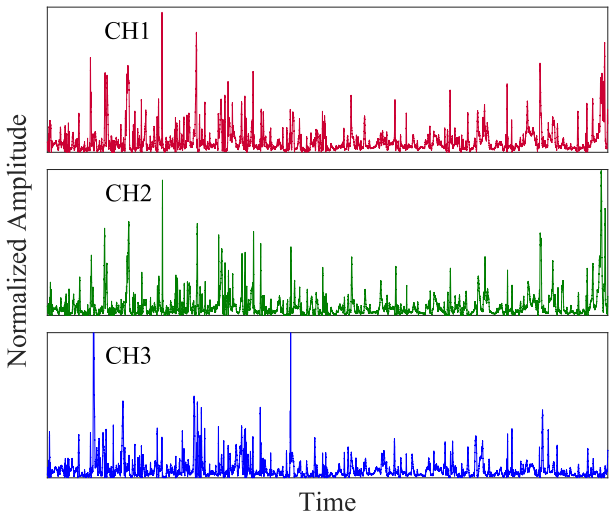

Fig. 5. Normalized amplitudes of different channel outputs.

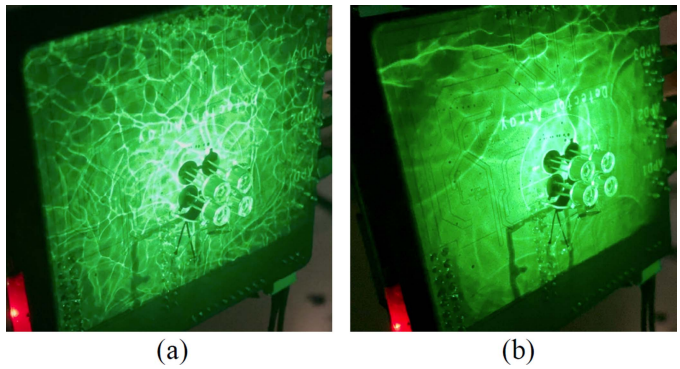

Fig. 6. Cross-section spot of arrived beam at receiving plane for (a) Case 1 and (b) Case 2.

from the conventional spot image of arrived beam undergoing atmospheric turbulence [23], a more evident stripe pattern can be observed for both cases. For the turbulence occurring near the APD array, the scale of the expanded light beam after traveling through the underwater channel is much larger than that of the generated turbulence eddies, which leads to a more random behavior of the arrived spill light as shown in Fig. 6(a). However, the scale of the generated turbulence eddies is similar to or larger than that of the narrow beam for Case 2, leading to a high probability for the beam passing through the same turbulence eddies and a large correlation across outputs of multiple detectors.

B. Communication Performances

Beginning from the typical scenario with lower correlation across multiple detectors, Fig. 7 shows the error vector amplitude

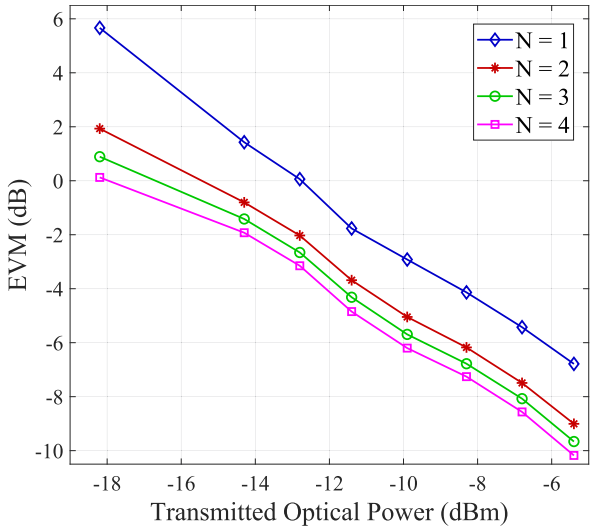

Fig. 7. EVM of the MRC scheme versus various transmitted optical power with different numbers of APDs for Case 1.

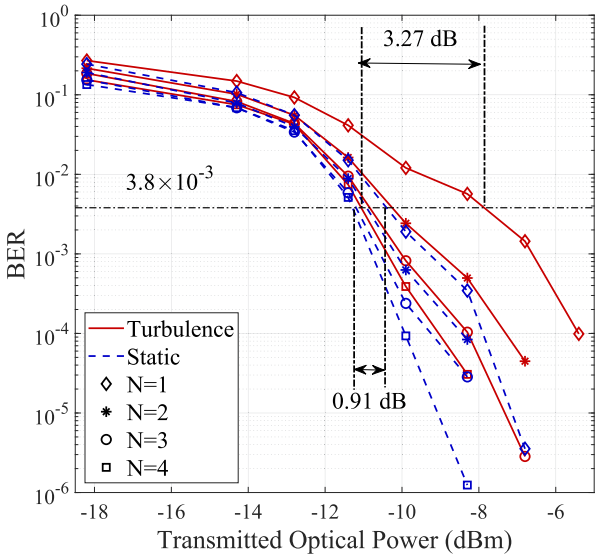

Fig. 8. BER of the MRC scheme versus the transmitted optical power for various numbers of detectors with or without turbulence for Case 1.

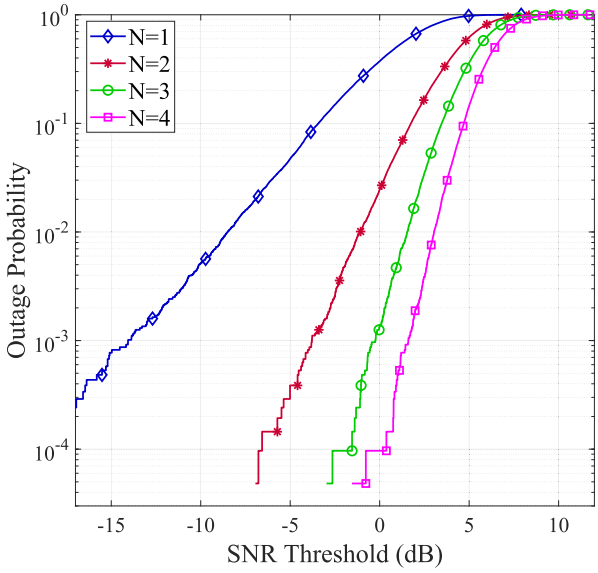

Fig. 9. Outage probability with the MRC scheme under various numbers of detectors for Case 1.

(EVM) which is a measure of the received signal quality [13], versus transmitted optical power adopting MRC scheme with different numbers of APDs in Case 1. Clearly, the EVM performance improves with the increasing of the transmitted optical power and a 2 dB optical power gain can be observed for $N = 2$ as compared to that of single APD. However, an optical power gain less than 1 dB can be obtained with N increasing from 2 to 3 and 3 to 4 due to non-negligible correlation across multiple APDs.

Fig. 8 shows the BER performance versus the transmitted optical power in Case 1 with weak correlation between different subchannel outputs. Obviously, a 0.91 dB optical power gain can be obtained given a forward-error-correction (FEC) limit of BER 3.8×10^{-3} for the MRC scheme with $N = 4$ as compared to single APD detector under static underwater channel. Besides, a 3.27 dB optical power gain can be observed for the MRC scheme with $N = 4$ as compared to single APD detector under turbulence channel, which reveals that a higher gain can be acquired by MRC due to the receiver diversity gain in mitigating the turbulence effect.

Moreover, Fig. 9 presents the outage probability versus SNR threshold with transmitted optical power -12.8 dBm for various numbers of MRC branches. Clearly, the outage probability utilizing multiple APDs significantly decreases as compared to that of single APD, which suggests that the receiver diversity can be leveraged to alleviate the probability of link interruption induced by turbulence.

To further describe the impact of the correlation across multiple detectors on the UOWC system performance, the similar experimental setup and measurement are conducted for turbulence generated at the location near the light source, while the average transmitted optical power is further increased to compensate the decreasing of the average received amplitude suggested in Fig. 3. Fig. 10 shows the BER performance of three subchannels and their paired combinations in Case 2 associated with

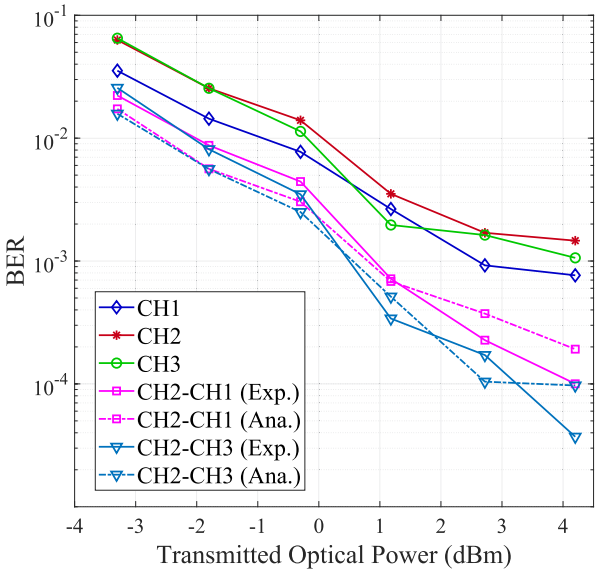

Fig. 10. BER performance versus the transmitted optical power under various subchannels and their optimal paired combinations for Case 2.

the proposed MRC scheme. Here, the correlation coefficients between CH2 and CH1, CH2 and CH3 are approximately 0.68 and 0.32, respectively. For comparison, analytical results for two paired subchannels are plotted by dashed curves, showing good agreement with corresponding experimental results. The BER of the MRC scheme combining the outputs of CH2 and CH3 outperforms that after combining the outputs of CH2 and CH1, even though the BER of the output of CH3 is worse than that of CH1. This observation suggests that stronger correlation between subchannels will lead to smaller combining gain. Thus, the detector spacing in the limited receiving area has to be properly optimized to achieve a good tradeoff between the power gain and diversity gain. Meanwhile, the analytical BER results are close to the experimental results, and a gap between

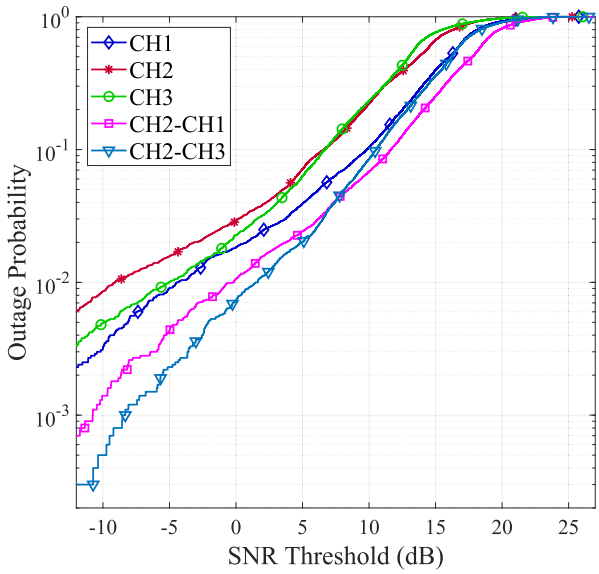

Fig. 11. Outage probability under various subchannels and their paired combinations for Case 2.

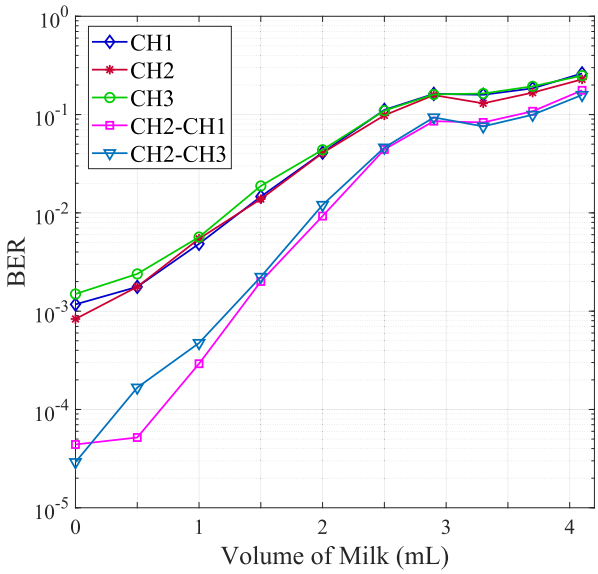

Fig. 12. BER performance versus the volume of added milk for Case 2.

analytical BER results and the experimental BER results can still be observed due to inaccurate channel estimation.

Fig. 11 shows the outage probability given different SNR thresholds with transmitted optical power −0.3 dBm. It can be seen that the outage probability of combined output is lower than that of single channel. However, the outage probability improvement introduced by the spatial diversity with strong channel correlation is apparently less than that with weak channel correlation, as observed by comparing Figs. 9 and 11.

To investigate the effect of turbidity, we conduct the experiment in Case 2 by placing a transparent acrylic container filled with turbid water in front of the receiver. Following Refs. [24], [25], [26], different water turbidities in the acrylic container are realized by mixing tap water of 28 L with concentrated milk of $0.5 \sim 4.0$ mL. Fig. 12 shows the BER under different volumes of added milk. It is observed that the BER increases with the volume of added milk, due to the increase of turbidity and attenuation coefficient.

V. Conclusion

In this paper, an experimental platform has been established to study the temperature-induced turbulence effect with the correlated SIMO channel for turbulence occurring at different locations. It is further shown that the spatial diversity can be leveraged to mitigate the effect of turbulence fading in a UOWC system and the optimal paired combinations can achieve a SNR gain above 3 dB over the single branch receiver at the BER of 10^{-3}. When the receiver elements failed to be placed sufficiently apart, the diversity gain will be reduced by the correlation within detectors. Thus, the detector spacing in the limited receiving area has to be properly optimized to achieve a good tradeoff between the power gain and diversity gain. Future work includes experiments in real long-distance scenarios, e.g., to create turbulence within the pool along the laser beam propagation path.

References

[1] C. Zhang et al., "3.8Gb/s PAM-4 UOWC system over a 2-m underwater channel enabled by a single-pixel 175-μm GaN-based mini-LED," *IEEE Photon. J.*, vol. 14, no. 3, Jun. 2022, Art. no. 7323207.

[2] C. Fei et al., "100-m/3-Gbps underwater wireless optical transmission using a wideband photomultiplier tube (PMT)," *Opt. Express*, vol. 30, no. 2, pp. 2326–2337, 2022.

[3] Y. Dai et al., "200-m/500-Mbps underwater wireless optical communication system utilizing a sparse nonlinear equalizer with a variable step size generalized orthogonal matching pursuit," *Opt. Exp.*, vol. 29, no. 20, pp. 32228–32243, 2021.

[4] J. Wang, C. Lu, S. Li, and Z. Xu, "100m/500Mbps underwater optical wireless communication using an NRZ-OOK modulated 520nm laser diode," *Opt. Exp.*, vol. 27, no. 9, pp. 12171–12181, 2019.

[5] C. Tu, W. Liu, W. Jiang, and Z. Xu, "First demonstration of 1Gb/s PAM4 signal transmission over a 130m underwater optical wireless communication channel with digital equalization," in *Proc. IEEE/CIC Int. Conf. Commun. China*, 2021, pp. 853–857.

[6] D. Chen, J. Wang, S. Li, and Z. Xu, "Effects of air bubbles on underwater optical wireless communication," *Chin. Opt. Lett.*, vol. 17, no. 10, 2019, Art. no. 100008.

[7] S. Jaruwatanadilok, "Underwater wireless optical communication channel modeling and performance evaluation using vector radiative transfer theory," *IEEE J. Sel. Areas Commun.*, vol. 26, no. 9, pp. 1620–1627, Dec. 2008.

[8] Y. Ata, H. Abumarshoud, L. Bariah, S. Muhaidat, and M. A. Imran, "Intelligent reflecting surfaces for underwater visible light communications," *IEEE Photon. J.*, vol. 15, no. 1, Feb. 2023, Art. no. 7300609.

[9] M. V. Jamali et al., "Statistical studies of fading in underwater wireless optical channels in the presence of air bubble, temperature, and salinity random variations," *IEEE Trans. Commun.*, vol. 66, no. 10, pp. 4706–4723, Oct. 2018.

[10] W. Jiang, W. Liu, and Z. Xu, "Experimental investigation of turbulence channel characteristics for underwater optical wireless communications," in *Proc. IEEE/CIC Int. Conf. Commun. China*, 2021, pp. 858–863.

[11] L. Bariah, M. Elamassie, S. Muhaidat, P. C. Sofotasios, and M. Uysal, "Non-orthogonal multiple access-based underwater VLC systems in the presence of turbulence," *IEEE Photon. J.*, vol. 14, no. 1, Feb. 2022, Art. no. 7308707.

[12] H. M. Oubei, R. T. ElAfandy, K. H. Park, T. K. Ng, M. S. Alouini, and B. S. Ooi, "Performance evaluation of underwater wireless optical communications links in the presence of different air bubble populations," *IEEE Photon. J.*, vol. 9, no. 2, Apr. 2017, Art. no. 7903009.

[13] W. Liu, Z. Ye, N. Huang, S. Li, and Z. Xu, "Multilevel polarization shift keying modulation for turbulence-robust underwater optical wireless communication," *Opt. Exp.*, vol. 31, no. 5, pp. 8400–8413, 2023.

[14] W. Liu, Z. Xu, and L. Yang, "SIMO detection schemes for underwater optical wireless communication under turbulence," *Photon. Res.*, vol. 3, no. 3, pp. 48–53, 2015.
[15] M. V. Jamali, J. A. Salehi, and F. Akhoundi, "Performance studies of underwater wireless optical communication systems with spatial diversity: MIMO scheme," *IEEE Trans. Commun.*, vol. 65, no. 3, pp. 1176–1192, Mar. 2017.
[16] P. Ramavath, A. Udupi, and P. Krishnan, "Experimental demonstration and analysis of underwater wireless optical communication link: Design, BCH coded receiver diversity over the turbid and turbulent seawater channels," *Microw. Opt. Technol. Lett.*, vol. 62, no. 6, pp. 2207–2216, 2020.
[17] X. Zhu and J. M. Kahn, "Free-space optical communication through atmospheric turbulence channels," *IEEE Trans. Commun.*, vol. 50, no. 8, pp. 1293–1300, Aug. 2002.
[18] M.-S. Alouini and M. K. Simon, "Dual diversity over correlated log-normal fading channels," *IEEE Trans. Commun.*, vol. 50, no. 12, pp. 1946–1959, Dec. 2002.
[19] Y. Tokgoz and B. D. Rao, "The effects of channel correlation on maximal ratio combining performance in the presence of cochannel interferers," in *Proc. IEEE Int. Conf. Acoust., Speech, Signal Process.*, 2003, pp. IV-377–IV-380.
[20] C. Chen and H. Yang, "Correlation between turbulence-impacted optical signals collected via a pair of adjacent spatial-mode receivers," *Opt. Exp.*, vol. 28, no. 10, pp. 14280–14299, 2020.
[21] W. Liu and Z. Xu, "APD nonlinearity and its impact on PAM-based visible light communication," *IEEE Commun. Lett.*, vol. 24, no. 5, pp. 1057–1061, May 2020.
[22] S. Benedetto, R. Gaudino, and P. Poggiolini, "Direct detection of optical digital transmission based on polarization shift keying modulation," *IEEE J. Sel. Areas Commun.*, vol. 13, no. 3, pp. 531–542, Apr. 1995.
[23] X. Yu et al., "2.5 Gbps free-space optical transmission between two 5G airship floating base stations at a distance of 12 km," *Opt. Lett.*, vol. 46, no. 9, pp. 2156–2159, 2021.
[24] Z. Pan, Y. Xiao, Y. Cao, L. Zhou, and W. Chen, "Optical data transmission through highly dynamic and turbid water using dynamic scaling factors and single-pixel detector," *Opt. Exp.*, vol. 30, no. 24, pp. 43480–43490, 2022.
[25] K. O. Amer, M. Elbouz, A. Alfalou, C. Brosseau, and J. Hajjami, "Enhancing underwater optical imaging by using a low-pass polarization filter," *Opt. Exp.*, vol. 27, no. 2, pp. 621–643, 2019.
[26] S. Stocker et al., "Broadband optical properties of milk," *Appl. Spectrosc.*, vol. 71, no. 5, pp. 951–962, 2017.